Available online at www.sciencedirect.com
SCIENCE DIRECT®
PERGAMON
International Journal of Heat and Mass Transfer 46 (2003) 3497–3509
International Journal of HEAT and MASS TRANSFER
www.elsevier.com/locate/ijhmt

Cocurrent turbulent mixed convection heat and mass transfer in falling film of water inside a vertical heated tube

M. Feddaoui *, A. Mir, E. Belahmidi

Groupe de Recherche sur l'Energie et la Thermique (GRETH), EST d'Agadir, B.P. 33/s, Morocco

Received 11 December 2001; received in revised form 2 January 2003

Abstract

A detailed numerical study has been conducted in order to analyse the combined buoyancy effects of thermal and mass diffusion on the turbulent mixed convection tube flows. Numerical results for air–water system are presented under different conditions. A low Reynolds number k–ε turbulent model is used with combined heat and mass transfer analysis in a vertical heated tube. The local heat fluxes, Nusselt and Sherwood numbers are reported to obtain an understanding of the physical phenomena. Predicted results show that a better heat transfer results for a higher gas flow Reynolds number Re, a higher heat flux q_w or a lower inlet water flow Γ_0. Additionally, the results indicate that the convection of heat by the flowing water film becomes the main mechanism for heat removal from the wall.

Keywords: Heat and mass transfer; Mixed convection; Vertical tube; Evaporation; Buoyancy influence; Turbulence modeling

1. Introduction

Simultaneous heat and mass transfer between a thin liquid film and gas/vapor stream are widely encountered in practice such as; the evaporative cooling for waste heat disposal, cooling towers and the protection of system components from a high temperature gas stream. The purpose of this article is to report on a study of combined buoyancy effects of thermal and mass diffusion on the turbulent mixed convection heat and mass transfer in vertical heated tube.

The turbulent mixed convection heat transfer and flow in vertical tube has been carried out by a number of investigators. Nakajima et al. [1] investigate the turbulent mixed convection between vertical parallel plates subject to different wall temperatures. They adopted a modified mixing length model to examine the effects of aiding and opposing buoyancy forces on fully turbulent forced convection. Recently, Tanaka et al. [2] applied a slight variant of the Jones and Launder [3] turbulence model against their data for heated ascending flow of nitrogen and found generally good agreement between measured and calculated Nusselt number. Cotton and Jackson [4] found that the low Reynolds number k–ε model of Launder and Sharma [5] (a re-optimisation of the Jones and Launder model [3]) for developing flow in a tube show close agreement with a range of experimental heat transfer data and flow profile measurements for air.

The detailed analysis, including transport processes in the flowing gas, was performed by Lin et al. [6] and Tsay and Yan [7]. They analysed the influence of wetted wall on laminar mixed convection heat and mass transfer in vertical ducts. In their analyses, the liquid film on the wetted wall was assumed to be extremely thin so that it was regarded as a boundary condition for heat and mass transfer only. Yan [8] published a study to investigate the turbulent mixed convection flow in a vertical channel under the simultaneous influence of the combined buoyancy forces of thermal and mass diffusion. A similar study was conducted by Fedorov et al. [9] to analyse the combined heat and mass transfer in an asymmetrically heated, parallel plates vertical channel.

As far as mixed convection heat and mass transfer including transport process in both gas flow and liquid

* Corresponding author.

0017-9310/03/$ - see front matter © 2003 Published by Elsevier Science Ltd.
doi:10.1016/S0017-9310(03)00129-7

Nomenclature

C_1, C_2	constants in production, sink terms of ε-equation
C_μ	constant in constitutive equation of k–ε model
c_p	specific heat [J kg^{-1} K^{-1}]
c_{pa}	specific heat of air [J kg^{-1} K^{-1}]
c_{pv}	specific heat of water vapour [J kg^{-1} K^{-1}]
D	mass diffusivity [m^2 s^{-1}]
d	diameter of the tube [m]
f_2	function in sink term of ε-equation
f_μ	function in constitutive equation of k–ε model
g	gravitational acceleration [m s^{-2}]
h_M	masse transfer coefficient [m s^{-1}]
h_T	heat transfer coefficient [W m^{-2} K^{-1}]
k	turbulent kinetic energy [m^2 s^{-2}]
$\dot{m}_I$	evaporating mass flux [kg m^{-2} s^{-1}]
$\dot{M}$	gas mass flow rate [kg m^{-1} s^{-1}]
Mr	dimensionless film evaporation rate (see Eq. 35)
M_a	molar mass of air [kg mol^{-1} K^{-1}]
M_v	molar mass of vapour [kg mol^{-1} K^{-1}]
Nu_ℓ	local Nusselt number of latent heat transport (see Eq. 26)
Nu_s	local Nusselt number of sensible heat transport (see Eq. 25)
Nu_z	overall Nusselt number (see Eq. 24)
p	mixture pressure [Pa]
p_d	dynamic pressure [Pa]
Pr	Prandtl number at inlet, v_0/α_0
q_w	wall heat flux [W m^{-2}]
q_I	total heat flux [W m^{-2}]
$q_{\ell I}$	latent heat flux [W m^{-2}]
q_{sI}	sensible heat flux [W m^{-2}]
r	co-ordinate in r-direction [m]
R	radius of the tube [m]
Re	Reynolds number of the gas stream, $u_0 d/v_0$
Re_L	inlet liquid film Reynolds number, $4\Gamma_0/(\pi d\mu_0)$
Re_t	turbulent Reynolds number, $k^2/(v\tilde{\varepsilon})$
Sc	Schmidt number at inlet, v_0/D_0
Sh_z	interfacial Sherwood number (see Eq. 27)
T	temperature [K]
T_{L0}	inlet liquid film temperature [K]
T_0	inlet temperature [K]
u	axial velocity [m s^{-1}]
v	radial velocity [m s^{-1}]
w	mass fraction of vapour
W	dimensionless mass fraction of vapour, $(w-w_0)/(w_I-w_0)$
y	normal distance from the wall, $R-r$ [m]
z	dimensional axial co-ordinate [m]
Z	dimensionless axial co-ordinate, z/d

Greek symbols

α	thermal diffusivity [m^2 s^{-1}]
Γ_0	inlet liquid mass flow rate [kg m^{-1} s^{-1}], $\int_{R-\delta_0}^{R}(2\pi r\rho u)_L\,dr$
δ_z	local liquid film thickness [m]
θ	dimensionless temperature, $(T-T_0)/(T_w-T_0)$
$\tilde{\varepsilon}$	rate dissipation of k [m^2 s^{-3}]
γ	latent heat of vapourisation [J kg^{-1}]
λ	thermal conductivity [W m^{-1} K^{-1}]
μ	dynamic viscosity [kg m^{-1} s^{-1}]
v	kinematics viscosity [m^2 s^{-1}]
ρ	density [kg m^{-3}]
ϕ	relative humidity at inlet
σ_t	turbulent Prandtl number
σ_w	turbulent Schmidt number
σ_k, σ_ε	turbulent Prandtl number for diffusion of k and ε

Subscripts

a	air
b	bulk quantity
I	condition at the gas–liquid interface
G	mixture (gas + vapour)
L	liquid film
0	condition at inlet
t	turbulent
v	vapour
w	condition at wall

film in vertical ducts is concerned, Yan [10] published a study to investigate the effect of finite film thickness on the laminar mixed convection heat and mass transfer in a vertical pipe. He found that the assumption of an extremely thin film is only valid for a system with a small liquid mass flow rate. The evaporative cooling of liquid film in natural convection channel flows was explored by Yan et al. [11,12] and in mixed convection tube flows by Feddaoui et al. [13]. Their results show that the liquid film cooling is mainly caused by latent heat transfer associated with its evaporation. Studies of combined heat and mass transfer in turbulent gas flow over a vaporizing liquid film was simultaneously performed by Shembharkar and Pai [14] and Baumann and Thiele [15]. In addition, Wongwises and Naphon [16] carried out an experimental and theoretical study of the heat and mass transfer characteristics for the vertical counter-current annular flow. A theoretical model based on a high

Reynolds number k–ε turbulence was proposed. Yan [17] numerically examined the effects of thermal and solutal buoyancy forces of combined heat and mass transfer in a vertical channel. In his study he applied a low Reynolds number k–ε turbulent model in the gas stream to predict the turbulent flow. Additionally He et al. [18] considered a vertical tube with liquid water film cooling. The gas flow was considered to be turbulent and the liquid film was assumed to be laminar.

Despite its importance in many engineering applications, the turbulent mixed convection heat and mass transfer in a vertical tube have not received much attention. This motivates the present work which examines the cocurrent turbulent convection heat and mass transfer in a vertical heated tube with thermal and solutal buoyancy effects.

2. Problem formulation

2.1. Physical model and assumption

The physical model under consideration and the coordinates are shown schematically in Fig. 1. The tube wall is subjected to a uniform heat flux. The liquid film is fed with an inlet liquid temperature T_{L0}, and inlet liquid mass flow rate Γ_0. The air–water mixture enters the tube at temperature T_0, and at constant velocity u_0. The flow is considered to be turbulent and steady. The following additional assumptions are made in the analysis:

1. The flow is considered to be incompressible and axisymmetric.
2. The thermodynamic and thermophysical properties of air and air–water vapor mixture are function of both local temperature and concentration. Complete details on the evaluation of these properties are given in Appendix A.
3. Radiation heat transfer, viscous dissipation and other secondary effects are negligible.
4. The thermodynamic equilibrium is assumed at the air–water film interface when computing the mass fraction of water vapor.
5. The Reynolds number of the water film flow is assumed to be lower than the critical value of $Re_{Lc} = 1500$ for laminar conditions quoted by Ueda and Tanaka [19].
6. The inertial terms are neglected in the momentum equation of the liquid film as compared with the diffusional term. Moreover, for the thin liquid film the axial transfers of momentum and energy are smaller than those in the radial direction [14,15,20]. The pressure gradient is also neglected.
7. The air–water interface is assumed smooth and without any waves on the surface on the water film.

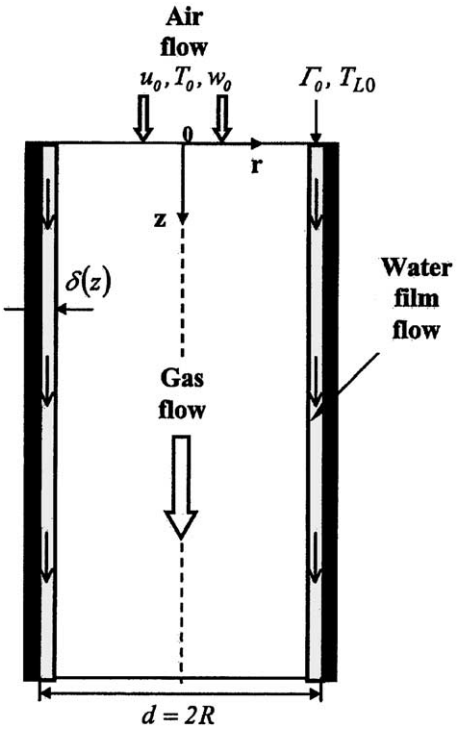

Fig. 1. Schematic diagram of the physical system.

2.2. Model equations

As a preliminary study, consideration is given to a system with low liquid mass flow rate that the liquid film may flow laminarly. As shown in the study of Dukler [21], the surface waves on a falling liquid film appear at $Re_L > 16$. Due to the complexity of the wave motion, an assumption of the time-wise steady film thickness used in numerous investigations [22,23], is also adopted in the present study. Therefore, the two-dimensional boundary layer flow in the liquid film is expressed by the following equations:

- Momentum

$$\frac{1}{r}\frac{\partial}{\partial r}\left(r\mu_L\frac{\partial u_L}{\partial r}\right) + \rho_L g = 0 \tag{1}$$

- Energy

$$\rho_L c_{pL} u_L \frac{\partial T_L}{\partial z} = \frac{1}{r}\frac{\partial}{\partial r}\left(r\lambda_L\frac{\partial T_L}{\partial r}\right) \tag{2}$$

With the above assumptions, the steady two-dimensional turbulent boundary layer flow in the gas side is governed by the following conservation equations:

- Continuity

$$\frac{\partial}{\partial z}(r\rho_G u_G) + \frac{\partial}{\partial r}(r\rho_G v_G) = 0 \tag{3}$$

- Momentum

$$\rho_G\left(u_G\frac{\partial u_G}{\partial z}+v_G\frac{\partial u_G}{\partial r}\right)=-\frac{dp_d}{dz}+\frac{1}{r}\frac{\partial}{\partial r}\left[r(\mu_G+\mu_{Gt})\frac{\partial u_G}{\partial r}\right]+(\rho_G-\rho_0)g \tag{4}$$

- Energy

$$\rho_G c_{pG}\left(u_G\frac{\partial T_G}{\partial z}+v_G\frac{\partial T_G}{\partial r}\right)=\frac{1}{r}\frac{\partial}{\partial r}\left[rc_{pG}\left(\frac{\mu_G}{Pr_G}+\frac{\mu_{Gt}}{\sigma_t}\right)\frac{\partial T_G}{\partial r}\right] \tag{5}$$

- Species concentration

$$\rho_G\left(u_G\frac{\partial w}{\partial z}+v_G\frac{\partial w}{\partial r}\right)=\frac{1}{r}\frac{\partial}{\partial r}\left[r\left(\frac{\mu_G}{Sc_G}+\frac{\mu_{Gt}}{\sigma_w}\right)\frac{\partial w}{\partial r}\right] \tag{6}$$

In the gas flow, the total absolute pressure is $p=p_d+p_0+\rho_0 gz$ thus the pressure gradient in Eq. (4) can be written as $dp/dz=(dp_d/dz)+\rho_0 g$. It is noted in Eq. (4) that the third term on the right-hand side represents the buoyancy forces due to the variations in temperature and concentration.

2.3. Turbulence model

For simulation of turbulence in the gas flow, a low Reynolds number k–ε turbulence model proposed by Launder and Sharma [5] is adopted to eliminate the usage of wall functions in the computation and thus to permit direct integration of the transport equations to the gas–liquid interface [4,18]. The local turbulent viscosity is determined from the solution of transport equations for the turbulent kinetic energy, k, and the energy dissipation rate, $\tilde{\varepsilon}$. Cast in cylindrical polar coordinates, the equations of the model are as follows.

2.3.1. Constitutive equation

Turbulent viscosity is expressed in terms of k and $\tilde{\varepsilon}$ by

$$\mu_{tG}=C_\mu f_\mu \rho_G k^2/\tilde{\varepsilon} \tag{7}$$

2.3.2. k-transport

$$\rho_G u_G\frac{\partial k}{\partial z}+\rho_G v_G\frac{\partial k}{\partial r}=\frac{1}{r}\frac{\partial}{\partial r}\left[r\left(\mu_G+\frac{\mu_{Gt}}{\sigma_k}\right)\frac{\partial k}{\partial r}\right]+\mu_{Gt}\left(\frac{\partial u_G}{\partial r}\right)^2-\rho_G(\tilde{\varepsilon}+D_\varepsilon) \tag{8}$$

2.3.3. ε-transport

$$\rho_G u_G\frac{\partial \tilde{\varepsilon}}{\partial z}+\rho_G v_G\frac{\partial \tilde{\varepsilon}}{\partial r}=\frac{1}{r}\frac{\partial}{\partial r}\left[r\left(\mu_G+\frac{\mu_{Gt}}{\sigma_\varepsilon}\right)\frac{\partial \tilde{\varepsilon}}{\partial r}\right]+C_1\frac{\tilde{\varepsilon}}{k}\mu_{Gt}\left(\frac{\partial u_G}{\partial r}\right)^2-\rho_G C_2 f_2\frac{\tilde{\varepsilon}^2}{k}+\frac{2\mu_G\mu_{Gt}}{\rho_G}\left(\frac{\partial^2 u_G}{\partial r^2}\right)^2 \tag{9}$$

2.3.4. Model constants and functions

The various constants and functions employed in the turbulence model are given as follows:

$$f_2=1-0.3\exp(-Re_t^2),\qquad f_\mu=\exp[-3.4/(1+Re_t/50)^2] \tag{10}$$

$$\tilde{\varepsilon}=\varepsilon-D_\varepsilon,\quad D_\varepsilon=2\nu_G\left(\frac{\partial k^{1/2}}{\partial r}\right)^2 \tag{11}$$

$$C_1=1.44,\quad C_2=1.92,\quad C_\mu=0.09,\qquad \sigma_k=1.0,\quad \sigma_\varepsilon=1.3,\quad \sigma_w=\sigma_t=0.9 \tag{12}$$

In the above, Re_t is the turbulent Reynolds number given by $Re_t=k^2/\nu\tilde{\varepsilon}$.

Because the flow involves combined heat and mass transfer, turbulent Prandtl and Schmidt numbers must be specified. Calculations with a constant value of $\sigma_t=0.9$ across the boundary layer show no pronounced effect on the heat transfer coefficient (i.e., Stanton number) and the temperature distributions [24]. Therefore, a value of $\sigma_w=\sigma_t=0.9$ is used in the calculations.

2.4. Boundary and interfacial matching conditions

The boundary conditions for this marching type problem are:

$$z=0:\ u_G=u_0,\quad T_G=T_0,\quad w=w_0,\qquad k_0=3/2(I_0u_0)^2,\quad \tilde{\varepsilon}_0=C_\mu k_0^{3/2}/0.03R \tag{13}$$

where I_0 is the turbulence intensity at the inlet of the tube.

$$r=0:\ \frac{\partial u_G}{\partial r}=0,\quad \frac{\partial T_G}{\partial r}=0,\quad \frac{\partial w}{\partial r}=0,\qquad \frac{\partial k}{\partial r}=0,\quad \frac{\partial \tilde{\varepsilon}}{\partial r}=0 \tag{14}$$

$$r=R:\ u_L=0,\quad \lambda_L\frac{\partial T_L}{\partial r}=q_w \tag{15}$$

The solution from the liquid side and gas side satisfy the following interfacial matching conditions ($r=R-\delta_z$):

(a) *Continuities of velocity and temperature*

$$u_I(z)=u_{G,I}=u_{L,I},\quad T_I(z)=T_{G,I}=T_{L,I} \tag{16}$$

(b) *Velocity of air–water vapor mixture at the interface*
The radial velocity component is non-zero due to the generation of vapor at the interface. Assuming that the gas–liquid interface is semi-permeable [25]. That is, the solubility of air in liquid film is negligibly small so that the air does not move radially at the interface, the velocity of the air–vapor mixture can be written as

$$v_{\mathrm{I}} = -\frac{(D + D_{\mathrm{t}})}{(1 - w_{\mathrm{I}})}\frac{\partial w}{\partial r} \tag{17}$$

(c) *The vapor fraction at the interface*
By assuming that the interface is at thermodynamic equilibrium and the air–water vapor mixture is an ideal gas mixture, the mass fraction of water vapor w_{I} can therefore be calculated using

$$w_{\mathrm{I}} = \frac{M_{\mathrm{v}} p_{\mathrm{v,I}}}{M_{\mathrm{a}}(p - p_{\mathrm{v,I}}) + M_{\mathrm{v}} p_{\mathrm{v,I}}} \tag{18}$$

where p and $p_{\mathrm{v,I}}$ are the total pressure and the vapor pressure at the interface, respectively. M_{a} and M_{v} are the molecular weights of air and vapor.

(d) *Continuity of shear stress*

$$\tau_{\mathrm{I}} = \left[\mu\frac{\partial u}{\partial r}\right]_{\mathrm{L,I}} = \left[(\mu + \mu_{\mathrm{t}})\frac{\partial u}{\partial r}\right]_{\mathrm{G,I}} \tag{19}$$

(e) *Heat balance at the interface implying*

$$\left[\lambda\frac{\partial T}{\partial r}\right]_{\mathrm{L,I}} = \left[(\lambda + \lambda_{\mathrm{t}})\frac{\partial T}{\partial r}\right]_{\mathrm{G,I}} + \dot{m}_{\mathrm{I}}.\gamma \tag{20}$$

where γ is the enthalpy of evaporation and $\dot{m}_{\mathrm{I}}$, the vapor generation rate ($= -\rho_{\mathrm{G}} v_{\mathrm{I}}$).
At the gas–liquid interface the values for u_{I} and T_{I} are calculated from Eqs. (19) and (20), also the interfacial blowing velocity and vapor concentration can be calculated from Eqs. (17) and (18) after the temperature at the interface is known. The total pressure at the interface is determined by assuming that the interface is in thermodynamic equilibrium, the relation between the saturated temperature and saturated pressure is described by Clausius–Clapeyron equation. A convenient set of correlation's used here for calculating the saturated pressure at a specified saturated temperature was developed by Fujii et al. [26], given by Antoin's correlation as

$$\log(p_{\mathrm{v,I}}/221.2) = -\{3.1323 + 3.116\times 10^{-6} \times (210 - T_{\mathrm{I}})^{2.066}\}\left(\frac{647.3}{T_{\mathrm{I}} + 273.15} - 1\right) \tag{21}$$

for 0 °C $< T_{\mathrm{I}} <$ 210 °C.

(f) *Turbulence parameters at the interface*
Since the water flow is assumed to be steady and laminar, we treat the water–gas interface as a solid wall with transpiration [18]; that is, we set the conditions:

$$k_{\mathrm{I}} = 0, \quad \tilde{\varepsilon}_{\mathrm{I}} = 0 \tag{22}$$

2.5. Heat and mass transfer parameters

The local heat exchange between the air stream and the liquid film depends on two related factors: the interfacial temperature gradient on the air side results in sensible convective heat transfer, and the evaporative mass transfer rate on the liquid film side results in latent heat transfer [9,27]. The total convective heat transfer rate from the film interface to the air stream can be expressed as follows:

$$\begin{aligned} q_{\mathrm{I}} &= q_{\mathrm{sI}} + q_{\ell\mathrm{I}} \\ &= \left[c_{\mathrm{p}}(\mu/Pr + \mu/\sigma_{\mathrm{T}})\frac{\partial T}{\partial r}\right]_{\mathrm{G,I}} \\ &\quad + \left[\frac{(\mu/Sc + \mu_{\mathrm{t}}/\sigma_{\mathrm{w}})}{(1 - w_{\mathrm{I}})}\frac{\partial w}{\partial r}\right]_{\mathrm{G,I}} \cdot \gamma \end{aligned} \tag{23}$$

For the purpose of generalizing the heat transfer results, the local Nusselt number along the gas–liquid interface is defined as

$$Nu_z = \frac{h_{\mathrm{T}}(2R)}{\lambda_{\mathrm{G}}} = \frac{q_{\mathrm{I}}(2R)}{\lambda_{\mathrm{G}}(T_{\mathrm{I}} - T_{\mathrm{b}})} = Nu_{\mathrm{s}} + Nu_{\ell} \tag{24}$$

where Nu_{s} and Nu_{ℓ} are the local Nusselt numbers for sensible and latent heat transfer, respectively, and are expressed as follows:

$$Nu_{\mathrm{s}} = \frac{q_{\mathrm{sI}}(2R)}{\lambda_{\mathrm{G}}(T_{\mathrm{I}} - T_{\mathrm{b}})} \tag{25}$$

$$Nu_{\ell} = \frac{q_{\ell\mathrm{I}}(2R)}{\lambda_{\mathrm{G}}(T_{\mathrm{I}} - T_{\mathrm{b}})} \tag{26}$$

Basing the local mass-transfer coefficient on the diffusive mass flux, the local Sherwood number is defined as:

$$Sh_z = \frac{h_{\mathrm{M}}(2R)}{D} = \frac{\dot{m}_{\mathrm{I}}(1 - w_{\mathrm{I}})(2R)}{\rho_{\mathrm{G}} D(w_{\mathrm{I}} - w_{\mathrm{b}})} \tag{27}$$

where the subscript b denote the bulk quantities, the local bulk temperature T_{b} and mass fraction w_{b} in the channel are, respectively, defined as follows:

$$T_{\mathrm{b}} = \int_0^{R-\delta_z} \rho_{\mathrm{G}} c_{\mathrm{pG}} r u_{\mathrm{G}} T_{\mathrm{G}}\,\mathrm{d}r \Big/ \int_0^{R-\delta_z} \rho_{\mathrm{G}} c_{\mathrm{pG}} r u_{\mathrm{G}}\,\mathrm{d}r \tag{28}$$

and

$$w_{\mathrm{b}} = \int_0^{R-\delta_z} \rho_{\mathrm{G}} r u_{\mathrm{G}} w\,\mathrm{d}r \Big/ \int_0^{R-\delta_z} \rho_{\mathrm{G}} r u_{\mathrm{G}}\,\mathrm{d}r \tag{29}$$

3. Numerical method

In view of the impossibility of obtaining an analytical solution for the non-linear coupled differential equations, the problem defined by the parabolic system of equations (1)–(6) with the appropriate boundary conditions are solved by a finite difference numerical scheme. A fully implicit numerical scheme in which the axial convection terms are approximated by the backward difference and the radial convection and diffusion terms by the central difference is employed to transform the governing equations into finite-difference equations. Each system of the finite-difference equations forms a tridiagonal matrix equation, which can be efficiently solved by the TDMA method [28]. In the centreline ($r = 0$) of the tube, the diffusional terms are singular. A correct representation can be found from an application of L'Hospital's rule.

3.1. Marching procedure

After specifying the flow and thermal conditions, the numerical solution is advanced forward and step by step as follows:

(1) For any axial location z, guess the values of $\mathrm{d}p_\mathrm{d}/\mathrm{d}z$ and δ_z.
(2) Solve the finite-difference forms of Eqs. (1) and (4) simultaneously for velocities u_L and u_G.
(3) Integrate numerically the continuity equation of the gas stream to find v_G:

$$v_\mathrm{G} = -\frac{1}{\rho_\mathrm{G}}\frac{1}{r}\frac{\partial}{\partial z}\int_0^r \rho_\mathrm{G} u_\mathrm{G} r\,\mathrm{d}r \tag{30}$$

(4) Solve the finite-difference forms of Eqs. (2) and (5) for temperatures T_L and T_G.
(5) Solve the finite-difference forms of Eq. (6) for mass fraction of vapor w.
(6) Solve the finite-difference forms of Eqs. (8) and (9) for turbulent kinetic energy and the energy dissipation rate, k and $\tilde{\varepsilon}$.
(7) Check the satisfaction of the overall conservation of mass in both gas flow and liquid film. If the following criteria:

$$\left|\int_0^{R-\delta_z} r\rho_\mathrm{G}u_\mathrm{G}\,\mathrm{d}r - \left[\frac{(R-\delta_0)^2}{2}\rho_0 u_0 - \int_0^z \rho_\mathrm{G} v_\mathrm{I}\,\mathrm{d}z\right]\right| \Big/ \frac{(R-\delta_0)^2}{2}\rho_0 u_0 < 10^{-4} \tag{31a}$$

and

$$\left|\Gamma_0 - \left[\int_{R-\delta_z}^{R}(r\rho u\,\mathrm{d}r)_\mathrm{L} - \int_0^z \rho_\mathrm{G} v_\mathrm{I}\,\mathrm{d}z\right]\right| \Big/ \Gamma_0 < 10^{-4} \tag{31b}$$

are met, then test the convergence of the velocity, temperature, turbulent kinetic energy and the dissipation of turbulent kinetic energy fields. If the maximum relative errors between two consecutive iterations satisfy the criterion:

$$|\psi_{i,j}^n - \psi_{i,j}^{n-1}|_\mathrm{max}/|\psi_{i,j}^n|_\mathrm{max} < 10^{-4} \tag{32}$$

where ψ represents the variables u, T, w, k and $\tilde{\varepsilon}$.

The solution for the current axial location is complete. Now if Eq. (32) is not simultaneously met, repeatedly solve the finite-difference equations for u, v, T, w, k and $\tilde{\varepsilon}$ in the gas stream and liquid film until the condition specified in Eq. (32) is fulfilled. If Eqs. (31) are not satisfied, adjust $\mathrm{d}p_\mathrm{d}/\mathrm{d}z$ and δ_z and repeat procedures 1–7 for the current axial location.

3.2. Velocity and pressure coupling

The correction of the pressure gradient and axial velocity profile at each axial station in order to satisfy the global mass flow constraint is achieved using a method proposed by Raithby and Schneider [29], described by Anderson et al. [30]. To illustrate, we will let $S = -\mathrm{d}p/\mathrm{d}z$. We make an initial guess for $(-\mathrm{d}p/\mathrm{d}z) = (-\mathrm{d}p/\mathrm{d}z)^*$ and calculate provisional velocities $(u_j^{n+1})^*$ and a provisional gas mass flow rate $(\dot{M}_i^{n+1})^*$. Due to the linearity of the momentum equation with frozen coefficients, the correct velocity at each point from an application of Newton's method would be

$$u_j^{n+1} = (u_j^{n+1})^* + \frac{\partial u_j^{n+1}}{\partial S}\Delta S \tag{33}$$

where ΔS is the change in the pressure gradient required to satisfy the global mass flow constraint. We define $u_{p,j}^{n+1} = \partial u_j^{n+1}/\partial S$. The difference equations are actually differentiated with respect to the pressure gradient (S) to obtain difference equations for $u_{p,j}^{n+1}$ which are tridiagonal in form. The coefficients for the unknowns in these equations will be the same as for the original implicit difference equations. The Thomas algorithm is used to solve the system of algebraic equations for $u_{p,j}^{n+1}$. The boundary conditions on $u_{p,j}^{n+1}$ must be consistent with the velocity boundary conditions. On boundaries where the velocity is specified, $u_{p,j}^{n+1} = 0$. The solution for $u_{p,j}^{n+1}$ is then used to compute ΔS by noting that $u_{p,j}^{n+1}\Delta S$ is the correction in velocity at each point required to satisfy the global mass flow constraint. Thus we can write:

$$\dot{M}_i^{n+1} - \dot{M}_i^n = 2\pi\Delta S\int_0^{R-\delta_z} r\rho u_{p,j}^{n+1}\,\mathrm{d}r \tag{34}$$

where the integral is evaluated by numerical means. The $\dot{M}_i^{n+1}$ in Eq. (34) is the known value specified by the initial conditions. The required value of ΔS is determined from Eq. (34). The correct values of velocity u_j^{n+1}

can then be determined from Eq. (33). The continuity equation is then used to determine v_j^{n+1}.

3.3. Grid pattern

The liquid film thickness δ_z decrease with z due to the film evaporation, therefore, during the downstream marching at each iteration, the finite difference computational grid used must comply with the variations of computation domains with z. This was accomplished by first locating the interface at every axial location, and then dividing the film and gas regions into NL and NJ points, respectively. The interface position has to be recalculated during iteration by satisfying the overall conservation of mass in the liquid film.

To obtain enhanced accuracy in the numerical computations, grids are chosen to be non-uniform in both axial and radial directions. Accordingly the grids are compressed towards the interface gas–liquid (the first node in the gas side should be located in the viscous sublayer at most less than one from the interface) and towards the entrance of the tube. The non-uniformity of the grid is described here in detail—each grid spacing is increased by a fixed percentage from the centreline of the tube in r direction and from the top of tube in z direction. This results is a geometric progression in the size of the spacing. The scheme maintains a constant ratio between two adjacent increments, $\Delta z_{i+1} = 1.04\Delta z_i$; in axial direction, $\Delta r_{j+1} = 0.99\Delta r_j$; in the liquid film and $\Delta r_{j+1} = 1.005\Delta r_j$; in the gas flow. Here j is the jth radial grid point.

During the program tests, solutions for typical case were obtained using different grid sizes to ensure that the solution is grid-independent. The results from the computation from various grids arrangement are given in Table 1. It is noted that the differences in the local Nusselt and Sherwood numbers from computations using either $201 \times 201 \times 41$ or $101 \times 101 \times 21$ grids are always less then 5%. Thus, to reduce the cost of computation, the grid $101 \times 101 \times 21$ is adequate for the calculations presented in this paper.

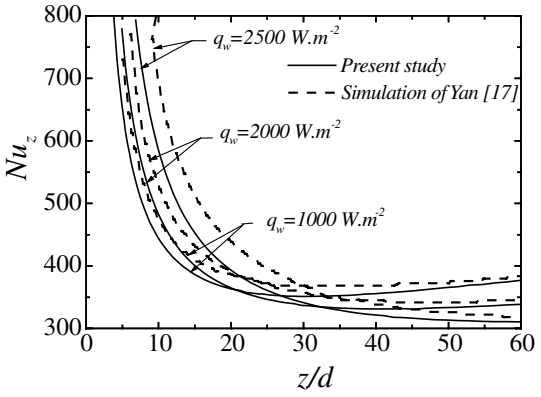

Fig. 2. Local Nusselt number Nu_z along the channel for $Re = 2 \times 10^4$.

Table 1
Comparisons of local interfacial Nusselt and Sherwood numbers for various grid arrangements and $q_w = 2500$ W m^{-2}, $\Gamma_0 = 0.02$ kg m^{-1} s^{-1}, $Re = 14000$

z/d	4.279	6.946	20.963	50.354	75.506	100.0
$51 \times 51 \times 11$						
Nu_z	902.29	510.77	235.51	194.89	206.21	228.05
Sh_z	39.68	36.91	33.59	32.31	31.89	31.73
$51 \times 101 \times 21$						
Nu_z	936.08	537.83	239.18	193.06	201.83	221.83
Sh_z	39.15	36.28	32.96	31.79	31.39	31.20
$101 \times 101 \times 21$						
Nu_z	926.27	540.26	239.22	192.60	201.63	221.98
Sh_z	38.89	36.33	32.97	31.79	31.38	31.22
$101 \times 151 \times 31$						
Nu_z	956.29	553.28	241.67	192.82	201.08	220.73
Sh_z	39.01	36.40	33.02	31.87	31.46	31.28
$201 \times 151 \times 31$						
Nu_z	967.46	561.74	242.92	194.93	201.25	220.79
Sh_z	39.11	36.49	33.02	31.89	31.45	31.29
$201 \times 201 \times 41$						
Nu_z	981.15	568.31	244.53	192.99	201.22	220.29
Sh_z	39.19	36.56	33.08	31.95	31.53	31.35

In Fig. 2 the present predictions of local Nusselt number Nu_z are compared with the prediction of Yan [17] for the case of liquid film evaporation in turbulent mixed convection flows in the vertical channel. In his study, a low Reynolds number k–ε turbulence model proposed by Myong and Kasagi [31] was used. The difference between the present analysis and the prediction of Yan is essentially due to the turbulence model used in two studies. Through these program test, the proposed numerical algorithm is considered to be suitable for the practical purpose.

4. Results and discussion

In order to examine the effects of flow conditions on the film cooling mechanism on mixed convection heat and mass transfer in a vertical tube, results are presented for water film evaporation. The following set of conditions are selected in the computation: the relative humidity of the ambient air is assigned as 50% at $T_0 = 20$ °C and 1 atm along a vertical tube with a radius $R = 0.03$ m. The liquid flow rate Γ_0 is chosen to be 0.01, 0.02 or 0.04 kg m^{-1} s^{-1}, and the inlet gas stream Reynolds number Re is 7000, 14 000 or 20 000.

The evolutions of the axial normalized velocity profiles along the tube are illustrated in Fig. 3 for various conditions. The imposed uniform inlet velocity profiles gradually adapts itself to a developed turbulent one. The temperature and mass fraction changes near the gas–liquid interface have significant effects on the corresponding velocity profiles, since the three fields are coupled. Thus, when the buoyancy effect becomes important at higher q_w or lower Re, at the exit of the tube, the negative velocities occurs for $y/R < 0.2$. In this case the flow is predicted to be partially laminarized. It is also noticed that an increase in q_w or a decrease in Re would result in higher axial normalized velocity. Thus a greater amount of water evaporates into the air for higher q_w or lower Re, and a larger buoyancy effects through thermal diffusion is obtained.

Figs. 4 and 5 present the axial temperature and mass fraction developments, respectively. For a given axial position, the temperature and concentration of the water film is relatively high at inlet. The fluid temperature and concentration increase monotonically with distance from the tube. A higher temperature distribution (Fig. 4) results for a higher q_w or a lower Re, this is due to the effects of buoyancy influences and mass diffusion, which appears under these conditions. From the gradient of concentration (Fig. 5) it is apparent that vapor is being transported away from the water film surface at all location along the tube. It is interesting to observe that both temperature and mass fraction develop in very similar fashion, except that the concentration boundary layer develops some what more rapidly than the thermal boundary layer does. In the case of low Reynolds number, the effect of buoyancy is very pronounced, and

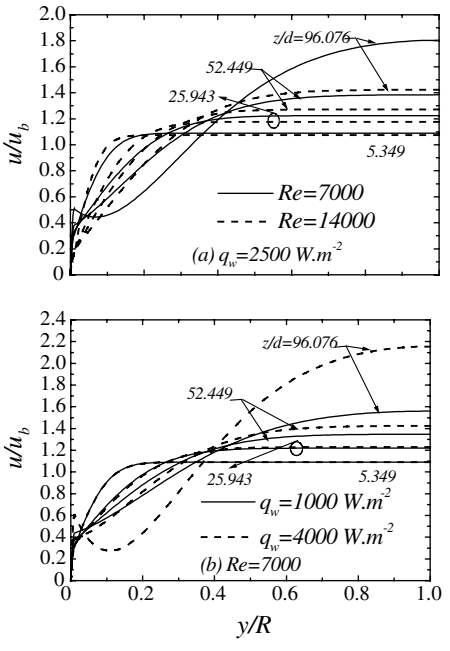

Fig. 3. Distributions of axial velocity profiles at different locations.

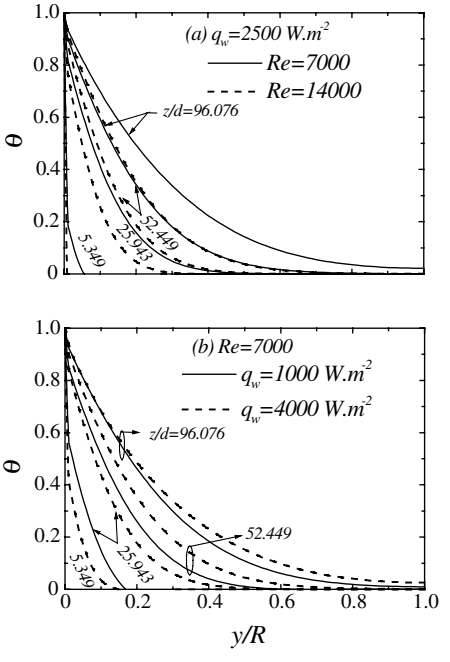

Fig. 4. Distributions of axial temperature profiles at different locations.

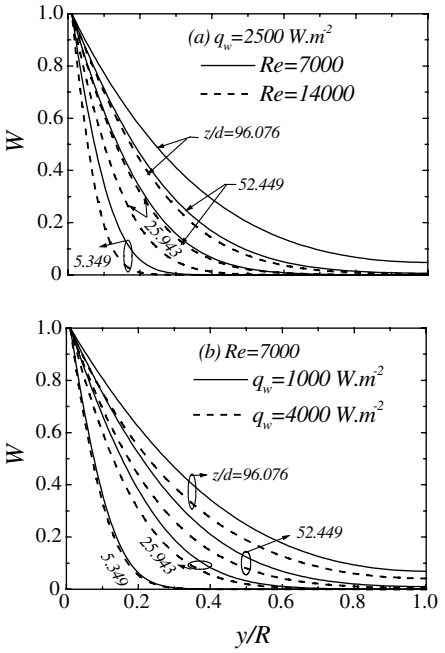

Fig. 5. Distributions of axial mass fraction profiles at different locations.

may lead to the laminarisation of the flow under certain conditions. This is clearly reflected in the value of Nusselt number. For that case, it is reduced to about one-third of that for forced convection under corresponding conditions of flow rate. Both the convective heat transfer from the interface and that due to evaporation are considerably impaired.

Fig. 6 shows the distributions of interfacial temperature and mass fraction of water vapor along the gas–liquid interface. The results indicate that the interfacial temperature increase monotonically in the flow direction. This feature is due to the fact that the water film absorbs sensible heat from the gas stream as the liquid film falls along the tube. As expected, the interfacial temperature is higher for a smaller inlet liquid mass flow rate. Therefore, the corresponding mass fraction, is also larger for systems with lower Γ_0.

The relative importance of the sensible and latent heat exchanges along the tube is illustrated in Fig. 7. It is noted that both the sensible and latent heat exchanges increase in the flow direction, but decrease with the liquid flow rate Γ_0. It is worth noting that at $\Gamma_0 = 0.01$ kg m^{-1} s^{-1}, q_s/q_w is always below 10%, but q_ℓ/q_w can be above 60%. Also, for a given liquid mass flow rate, the

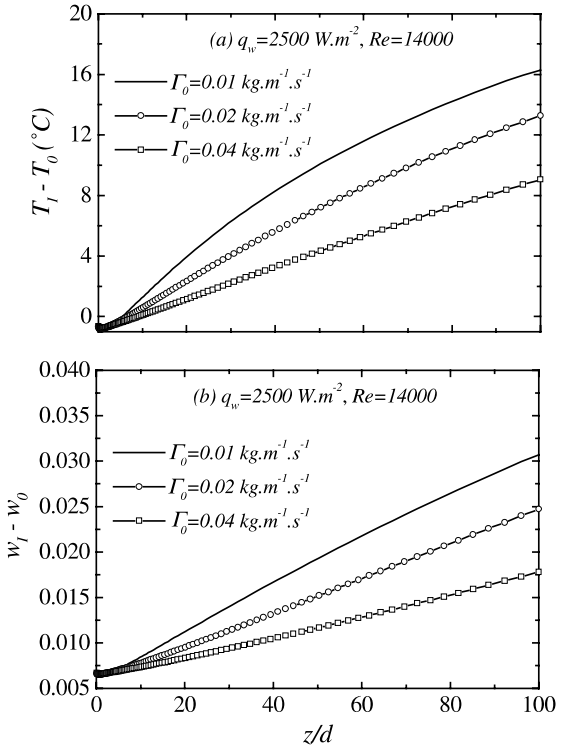

Fig. 6. Axial distributions of interfacial temperature and mass fraction.

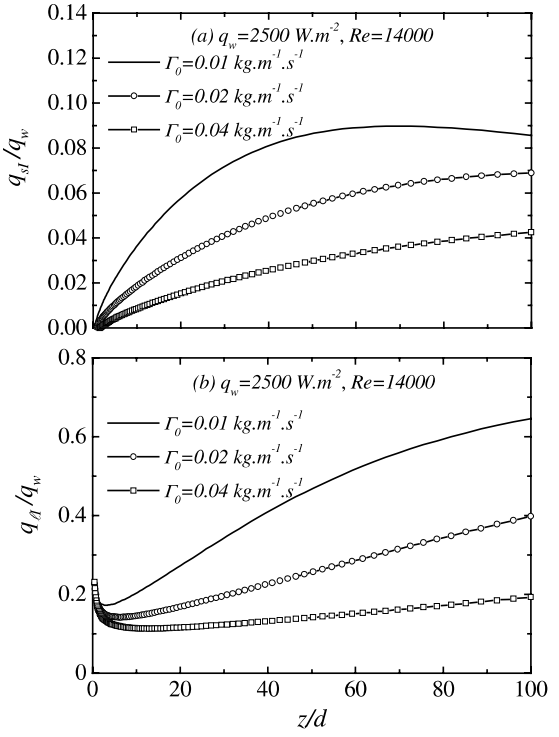

Fig. 7. Distributions of local dimensionless heat transfer rates along the tube: (a) interfacial sensible heat flux; (b) interfacial latent heat flux.

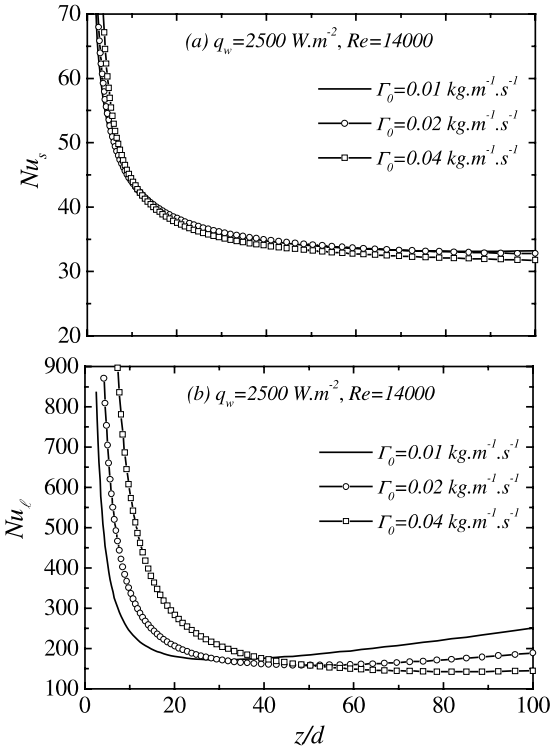

Fig. 8. Effects of liquid mass flow rate on the interfacial Nusselt numbers: (a) sensible heat Nusselt number; (b) latent heat Nusselt number.

latent heat exchange is about five times larger than the sensible heat exchange.

For more detailed analysis of heat and mass transfer characteristics at the interface, the variation of local Nusselt numbers of sensible and latent heat flux at the interface are shown in Fig. 8 for various inlet liquid mass flow rate. A slight smaller Nu_s is noted for a higher Γ_0 at the exit of the tube. Also shown from Fig. 8(b) that near the entrance ($z/d < 25$) a larger latent Nusselt number results for a lower inlet liquid mass flow rate, but as the flow goes downstream ($z/d > 40$) the reverse trend is noticed. This is due to the larger shearing effect created by the falling liquid film for a larger Γ_0. These results clearly indicate that the magnitude of Nu_ℓ is much larger than that of Nu_s, implying that the heat transfer resulting from latent heat exchange is much more effective.

The distributions of the interfacial mass evaporation rate and Sherwood number are presented in Fig. 9 for various Γ_0 to illustrate the mass transfer characteristics. A reduction in the film flow rate causes a greater film evaporation and $\dot{m}_1$ increase with z/d in the downstream region. These outcomes apparent result from the higher interface temperature at smaller Γ_0. The change in the flow rate has a smaller influence on the Sherwood number variations.

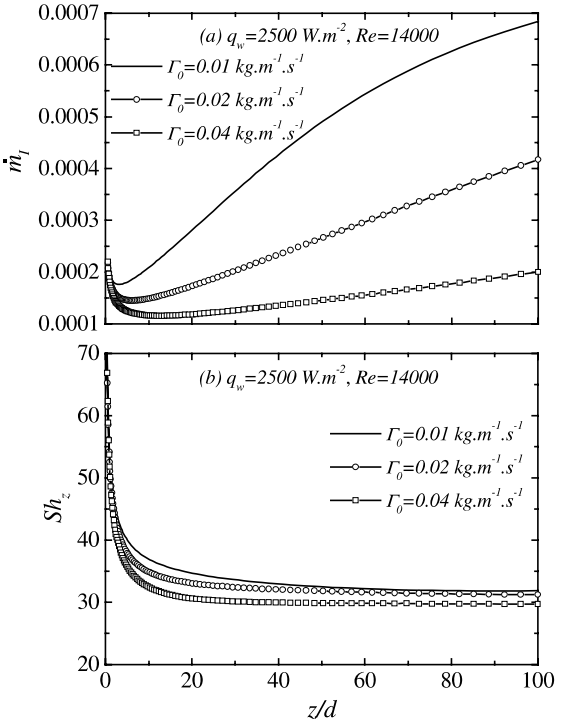

Fig. 9. Effects of liquid mass flow rate on the interfacial mass evaporation rate and Sherwood number distributions.

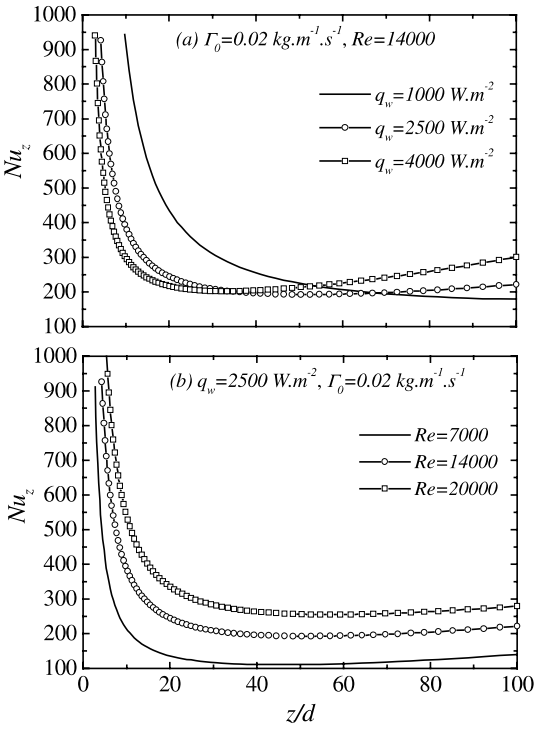

Fig. 10. Effects of wall heat flux q_w and Reynolds number of gas stream Re on the interfacial Nusselt number.

Fig. 10 gives the influence of the wall heat flux q_w and inlet Reynolds number of the gas stream Re on the distributions of the interfacial Nusselt number Nu_z. A larger Nu_z results for systems having a lower wall heat flux, but at the exit of the tube ($z/d > 70$) the reverse trend is noticed. Fig. 10(b) shows that Nu_z is larger for a higher Re, which implies that heat transfer is more effective in forced convection. This confirms the general concept that, for turbulent forced convection, the heat transfer is large for a higher Re.

It is of interest to investigate the effects of the wall heat flux and inlet Reynolds number on the mass transfer coefficients. Fig. 11 shows that near the entrance, Sh_z converges to a single constant value of 31.25. The Sherwood number is slightly influenced by the change in the wall heat flux (Fig. 11(a)). The results in Fig. 11(b) indicate that a larger Sh_z is noted for systems with a higher Re. This outcomes apparently results from the large interfacial evaporating rate for a higher Re, which in turn results in a larger Sherwood number Sh_z. This is due to the larger evaporating (blowing) effect along the gas–liquid interface.

In order to quantify the film evaporation a dimensionless accumulated mass evaporation rate Mr is introduced.

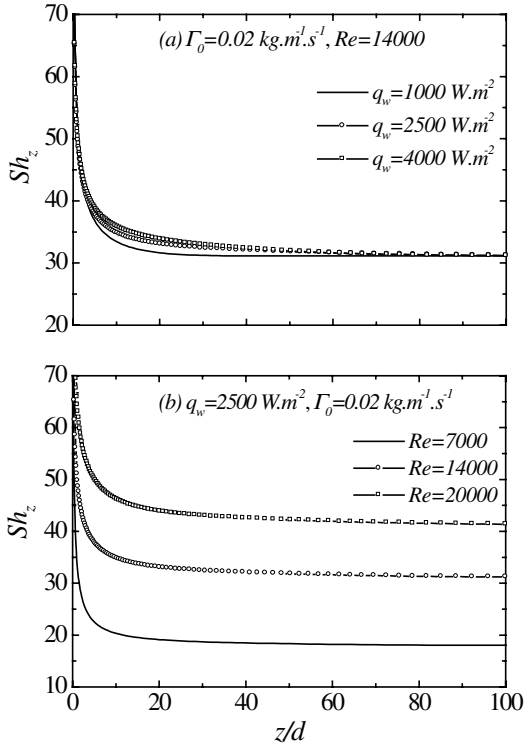

Fig. 11. Effects of wall heat flux q_w and Reynolds number of gas stream Re on the variations of Sherwood number.

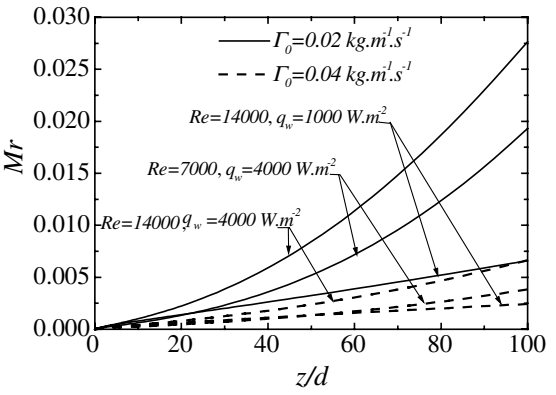

Fig. 12. Distributions of dimensionless accumulated evaporation rate Mr along the tube.

$$\mathrm{Mr} = \int_0^z \dot{m}_\mathrm{I}\,\mathrm{d}z \Big/ \Gamma_0 \tag{35}$$

The distribution of Mr for various cases are depicted in Fig. 12. The larger film evaporation is found for systems for higher q_w or higher Reynolds number Re. Also mentioning that a reduction in the inlet liquid film cause a greater film evaporation and Mr increase with z/d as the flow goes downstream. It is interesting to note that the largest accumulated mass evaporation rate Mr is about 3%. This clearly indicates the larger latent heat transport in connection with the greater liquid film evaporation.

5. Conclusion

The turbulent mixed convection heat and mass transfer in a vertical tube has been numerically studied by solving the respective governing equations for the liquid film and the gas stream coupled through the interfacial matching conditions. The effects of the inlet liquid flow rate Γ_0, wall heat fluxes q_w and gas stream Reynolds number Re on the momentum heat and mass transfer in the flow are investigated in detail. Based on the numerical results obtained, the main conclusions from the study are summarized as follows:

1. The Launder and Sharma turbulence model is generally able to respond well to the influences present on turbulence under the mixed convection prevailing in the complex combined heat and mass situation considered in this study.
2. The interfacial temperature and water vapor concentration is higher for a smaller inlet liquid flow rate Γ_0.
3. A larger heat and mass transfer results for systems with larger q_w or lower Re, this brought by the greater film evaporation and the larger buoyancy effects.

4. The magnitude of latent heat Nusselt number Nu_ℓ is much larger than that of sensible Nusselt number Nu_s. This implies that heat transfer along the gas–liquid interface is dominated by the latent heat transfer in conjunction with the liquid film evaporation.
5. The convection of heat by the flowing liquid film becomes the main mechanism for heat removal from the heated tube.

Appendix A

The properties of air, water vapour, their mixture and liquid water are calculated by the following formulas [26]:

Air: component 2

$$\mu_2 = 1.488 \times 10^{-6} \cdot T^{1.5}/(118 + T) \quad (\mathrm{kg/m\,s}) \tag{A.1}$$

$$\lambda_2 = 1.195 \times 10^{-3} \cdot T^{1.6}/(118 + T) \quad (\mathrm{W/m\,K}) \tag{A.2}$$

$$C_{p_2} = (1 + 2.5 \times 10^{-10} \cdot T^3) \times 10^3 \quad (\mathrm{J/kg\,K}) \tag{A.3}$$

Water vapour: component 1

$$\mu_1 = [8.02 + 0.0407(T - 273.16)] \times 10^{-6} \quad (\mathrm{kg/m\,s}) \tag{A.4}$$

$$\lambda_1 = [1.87 + 0.65 \times 10^{-3}(T - 273.16)^{9/7} + 5.7 \times 10^{-13}(T - 273.16)^{5.1}] \times 10^2 \quad (\mathrm{W/m\,K}) \tag{A.5}$$

$$C_{p_2} = 1.863 \times 10^3 + 1.65 \times 10^{-3}(T - 273.16)^{2.5} + 1.2 \times 10^{-18}(T - 273.16)^{8.5} \quad (\mathrm{J/kg\,K}) \tag{A.6}$$

Mixture (*Air* + *Water vapour*):

Density:

Under the assumption that the mixture of gas and water vapour behaves like a perfect gas, the density of the mixture can then be evaluated by the following relation:

$$\rho = p \Big/ \left[RT \left(\frac{w}{M_1} + \frac{1-w}{M_2} \right) \right] = \frac{12.0279p}{T\left(\frac{w}{M_1} + \frac{1-w}{M_2}\right)} \quad (\mathrm{kg/m^3}) \tag{A.7}$$

where the molecular weights of air and water vapour are $M_2 = 28.96$ (kg/K mol) and $M_1 = 18.02$ (kg/K mol), respectively.

$$\mu = \frac{\mu_1}{1 + \left(\frac{x_2}{x_1}\right)\phi_{12}} + \frac{\mu_2}{1 + \left(\frac{x_1}{x_2}\right)\phi_{21}} \quad (\mathrm{kg/m\,s}) \tag{A.8}$$

where x_1 and x_2 are the mole fractions of air and water vapour, respectively.

$$\phi_{ij} = \frac{[1 + (\mu_i/\mu_j)^{0.5}(M_j/M_i)^{0.25}]^2}{[8(1 + M_i/M_j)]^{0.5}} \tag{A.9}$$

$$\lambda = \frac{\lambda_1}{1 + \left(\frac{x_2}{x_1}\right)\phi_{12}} + \frac{\lambda_2}{1 + \left(\frac{x_1}{x_2}\right)\phi_{21}} \quad (\mathrm{W/m\,K}) \tag{A.10}$$

where ϕ_{12} and ϕ_{21} are identified to those that appeared in the viscosity equation (A.8).

$$C_p = C_{p_1} w_1 + C_{p_2}(1 - w_1) \quad (\mathrm{J/kg\,K}) \tag{A.11}$$

$$D = 8.07 \times 10^{-10} \cdot T^{1.833} \quad (\mathrm{m^2/s}) \tag{A.12}$$

Liquid water

$$\rho_L = \frac{10^3}{1 + 8.7 \times 10^{-6}(T - 273.16)^{1.85}} \quad (\mathrm{kg/m^3}) \tag{A.13}$$

$$\mu_L = 2.4 \times 10^{-5} \times 10^C \quad (\mathrm{kg/m\,s}) \tag{A.14}$$

where

$$C = \frac{251}{135 + (T - 273.16)}$$

$$\lambda_L = 0.6881 - 4 \times 10^{-6}(408.16 - T)^{2.1} \quad (\mathrm{W/m\,K}) \tag{A.15}$$

$$C_{p_L} = 4.179 \times 10^3 + 7.9 \times 10^{-5}(T - 283.16)^{2.9} \quad (\mathrm{J/kg\,K}) \tag{A.16}$$

In the above equations the units for temperature and pressure are Kelvin and bars, respectively.

References

[1] M. Nakajima, K. Fukai, H. Ueda, T. Mizushinal, Buoyancy effect of turbulent transport in combined free and forced convection between vertical parallel plates, Int. J. Heat Mass transfer 23 (1980) 1325–1336.
[2] H. Tanaka, S. Marayama, S. Hatano, Combined forced and natural convection heat transfer upward flow in a uniformly heated vertical pipe, Int. J. Heat Mass transfer 30 (1987) 165–174.
[3] W.P. Jones, B.E. Launder, The prediction of laminarization with a two-equation model of turbulence, Int. J. Heat Mass transfer 15 (1972) 301–314.
[4] M.A. Cotton, J.D. Jackson, Vertical tube air flows in the turbulent mixed convection regime calculated using a low-Reynolds-number $k \sim \varepsilon$ model, Int. J. Heat Mass transfer 33 (1990) 275–286.
[5] B.E. Launder, B.I. Sharma, Application of the energy-dissipation of turbulence to calculation of low Reynolds number flow near a spinning disc, Lett. Heat Mass transfer 1 (1974) 131–138.
[6] T.F. Lin, C.J. Chang, W.M. Yan, Analysis of combined buoyancy effects of thermal and mass diffusion on laminar forced convection heat transfer in a vertical tube, J. Heat Transfer 110 (1988) 337–344.

[7] H.C. Tsay, W.M. Yan, Binary diffusion and heat transfer in laminar mixed convection channel flows with uniform wall heat flux: extremely thin film thickness, Wärm und Stoffübertragung 26 (1990) 23–31.
[8] W.M. Yan, Turbulent mixed convection heat and mass transfer in wetted channel, J. Heat Transfer 117 (1995) 229–233.
[9] A.G. Fedorov, R. Viskanta, A.A. Mohamad, Turbulent heat and mass transfer in asymmetrically heated, vertical parallel-plate channel, Int. J. Heat Fluid Flow 18 (1997) 307–315.
[10] W.M. Yan, Binary diffusion and heat transfer in mixed convection pipe flows with film evaporation, Int. J. Heat Mass Transfer 36 (1993) 2115–2123.
[11] W.M. Yan, T.F. Lin, Y.L. Tsay, Evaporative cooling of liquid film in through interfacial heat and mass transfer in a vertical channel: I—Experimental study, Int. J. Heat Mass Transfer 34 (1991) 1105–1111.
[12] W.M. Yan, T.F. Lin, Evaporative cooling of liquid film in through interfacial heat and mass transfer in a vertical channel: II—Numerical study, Int. J. Heat Mass Transfer 34 (1991) 1113–1124.
[13] M. Feddaoui, E. Belahmidi, A. Mir, A. Bendou, Numerical study of the evaporative cooling of liquid film in laminar mixed convection tube flows, Int. J. Thermal Sci. 40 (2001) 1011–1020.
[14] T.R. Shembharkar, B.R. Pai, Prediction of film cooling with a liquid coolant, Int. J. Heat Mass Transfer 29 (1986) 899–908.
[15] W.W. Baumann, F. Thiele, Heat and mass transfer in evaporating two-component liquid film flow, Int. J. Heat Mass Transfer 33 (1990) 273–367.
[16] S. Wongwises, P. Naphon, Heat-mass transfer and flow characteristics of two-phase counter-current annular flow in vertical pipe, Int. Comm. Heat Mass Transfer 25 (1998) 819–829.
[17] W.M. Yan, Effect of film vaporization on turbulent mixed convection heat and mass transfer in vertical channel, Int. J. Heat Mass Transfer 38 (1995) 713–722.
[18] S. He, P. An, J. Li, J.D. Jackson, Combined heat and mass transfer in uniformly heated vertical tube with water film cooling, Int. J. Heat Fluid Flow 19 (1998) 401–417.
[19] T. Ueda, H. Tanaka, Measurement of velocity, temperature and velocity fluctuation distributions in liquid films, Int. J. Multiphase Flow 2 (1975) 261–272.
[20] K. Suzuki, Y. Hagiwara, T. Sato, Heat transfer and flow characteristics of two-phase two-component annular flow, Int. J. Heat Mass Transfer 26 (1983) 597–605.
[21] A.E. Dukler, Characterization, effects and modeling of the wavy gas–liquid interface, Prog. Heat Mass Transfer 6 (1972) 207–234.
[22] S.M. Yih, J.L. Liu, Prediction of heat transfer in turbulent falling liquid films with or without interfacial shear, AIChE J. 29 (1983) 903–909.
[23] M.H. Chun, S.J. Park, Effect of turbulence model and interface shear on heat transfer in turbulent falling liquid films, Int. Comm. Heat Mass Transfer 22 (1995) 1–12.
[24] T. Cebeci, Eddy viscosity distribution in thick axisymmetric turbulent boundary layers, J. Fluid Eng. 95 (1973) 319–326.
[25] E.R.G. Eckert, R.M. Drake, Analysis of Heat and Mass Transfer, McGraw-Hill, New York, 1972.
[26] T. Fujii, Y. Kato, K. Mihara, Expressions of transport and thermodynamic properties of air, stream and water, Sei San Ga Ken Kyu Jo, Report No. 66, Kyu Shu Dai Gaku, Kyu Shu, Japan, 1977, pp. 81–95.
[27] J.L. Manganaro, O.T. Hanna, Simultaneous energy and mass transfer in the laminar boundary with large mass transfer rates toward the surface, AIChE J. 16 (1970) 204–211.
[28] S.V. Patankar, Numerical Heat Transfer and Fluid Flow, Hemisphere/McGraw-Hill, New York, 1980, Chapter 4, pp. 52–53.
[29] G.D. Raithby, G.E. Schneider, Numerical solutions of problems in incompressible fluid flow: treatment of the velocity–pressure coupling, Numer. Heat Transfer 2 (1979) 417–440.
[30] D.A. Anderson, J.C. Tannehill, R.H. Pletcher, Computational Fluid Mechanics and Heat Transfer, Hemisphere/McGraw-Hill, New York, 1984.
[31] H.K. Myong, N. Kasagi, A new approach to the improvement of k–ε turbulence model for wall-bounded shear flow, JSME Int. J. 33 (1990) 63–72.